Macromolecules

Article

pubs.acs.org/Macromolecules

Phase Behaviors of Side-Chain Liquid Crystalline Polyacetylenes with Different Length of Spacer: Where Will the Decoupling Effect Appear?

Zhen-Qiang Yu,*[,†] Ting-Ting Li,[†] Zhe Zhang,[†] Jia-Hao Liu,[‡] Wang Zhang Yuan,[§] Jacky W. Y. Lam,[⊥] Shuang Yang,[‡] Er-Qiang Chen,*[,‡] and Ben Zhong Tang*[,⊥]

[†]Shenzhen Key Laboratory of Functional Polymers, School of Chemistry and Chemical Engineering, Shenzhen University, Shenzhen 518060, China

[‡]Beijing National Laboratory for Molecular Sciences, Department of Polymer Science and Engineering and the Key Laboratory of Polymer Chemistry and Physics of the Ministry of Education, College of Chemistry and Molecular Engineering, Center for Soft Matter Science and Engineering, Peking University, Beijing 100871, China

[§]School of Chemistry and Chemical Engineering, Shanghai Jiao Tong University, Shanghai 200240, China

[⊥]Department of Chemistry, The Hong Kong University of Science & Technology, Clear Water Bay, Kowloon, Hong Kong China

Supporting Information

ABSTRACT: Phase structures and transitions of a series of biphenyl containing side-chain liquid crystalline polyacetylenes (SCLCPAs) with different length of spacer and alkyl tail, poly((*m* + 2)-{[(4′-alkyloxy-4-biphenylyl)carbonyl]oxy}-1-yne) [P-*m*,7 (*m* = 4, 5, 8), P-*m*,5 (*m* = 9), P-*m*,5[L] (*m* = 3, 9), *m* is the number of methylene units in the spacer], were studied by differential scanning calorimeter, polarized light microscopy, one- and two-dimensional wide-angle X-ray diffraction. It is revealed that phase structures of the samples are strongly dependent on the lengths of spacer and alkyl tail. The samples with short spacer (*m* ≤ 4) render the molecular shape of sheet-like due to the strong coupling between the backbone and the biphenyl groups on side-chains. They form highly ordered smectic phase with an additional ordering on the subnanometer scale (SmX[o]) at low temperatures. For *m* > 5, P-*m*,7 exhibits the low-temperature phase of smectic B (SmB), while P-9,5 and P-9,5[L] form smectic E (SmE). As the long spacers adopt more *gauche* conformations to satisfy the ordered packing of biphenyl groups, the coupling of main- and side-chain is relieved. Among the samples studied, P-5,7 is unique, which can retain the sheet-like shape but form the SmB structure based on a fully interdigitated packing manner. Therefore, the spacer length of *m* = 5 sets the boundary between coupling and decoupling of the backbone and side-chains. Phase transition sequences of the SCLCPAs studied are also found to be influenced clearly by varying the spacer and tail lengths.

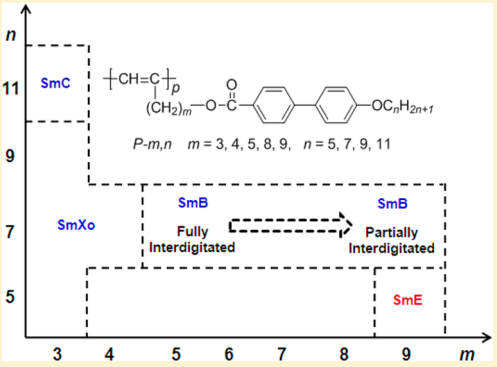

INTRODUCTION

From the viewpoint of molecular design, "flexible spacer" proposed by Finkelmann and Ringsdorf has been playing an important role in liquid crystal (LC) phase formation of the side-chain liquid crystalline polymers (LCPs).[1,2] That is, insertion of flexible spacers between the backbone and the mesogenic groups can effectively decouple the dynamics of both the components. As a result, the LC phases such as nematic and smectic of side-chain LCPs can appear easily when calamitic mesogens are incorporated into the side-chains. With regard to smectic structures of most side-chain LCPs, it is considered that parallel packing of the mesogens, which are usually chemically incompatible with the main-chain, can result in a microphase-separated structure containing different sublayers. The flexible main-chains (e.g., polyethylene) can form the amorphous sublayers on the both side of the mesogen sublayer, which can adjust their conformation to adapt the ordered packing of mesogens. In this case, the LC properties of the side-chain LCPs are more dependent on the LC properties of mesogens on side chains. For the side-chain LCPs with (semi)rigid backbones, the main-chain sublayer shall still exist in their smectic phases. However, more attention should be paid to the interplay of main- and side-chain. Since the rigid main-chain with reduced mobility is hard to vary its conformation, one may anticipate that they will have a negative impact on the LC ordering of side-chains. On the other hand, it is also possible that the (semi)rigid backbone bearing its own anisotropic shape can also involve into the LC structure formation, leading to some interesting LC behavior based on

Received: April 2, 2015
Revised: April 6, 2015
Published: April 15, 2015

DOI: 10.1021/acs.macromol.5b00692
Macromolecules 2015, 48, 2886−2893

cooperative contributions from both the main- and side-chain which are linked through a spacer.

Substituted polyacetylenes (PAs),[3−6] one of the most typical polymers with (semi)rigid backbone, have attracted considerable interest because of their unique properties such as semiconductivity,[6,7] liquid crystallinity,[8,9] gas permeability,[10,11] helix formation,[12−15] nonlinear optical properties,[16,17] optical electronics,[18,19] and also dispersion and alignment of carbon nanotubes.[20,21] Incorporation of mesogenic groups into the side-chains may result in side-chain liquid crystalline polyacetylenes (SCLCPAs),[8,9,22] of which the synthesis, properties, and phase behaviors have been widely investigated in the past decades.[23−45] When dealing with the phase structure formation of SCLCPAs, we must know what role the (semi)rigid PA backbone plays in guiding the molecules packing into condensed state.[22] Owning to the advances of synthetic researches, the stereostructure of SCLCPAs can be well controlled by selecting proper catalysts and polymerization conditions. The *cis*-PA backbone, particularly the *cis*-cisoidal one, can render helical conformation, leading to a cylindrical shape of the polymer. Cylinder-like SCLCPAs can form hexagonal or rectangular columnar phase,[46−48] wherein the PA main-chains in fact determine the LC phase structures. For some *cis*-transoidal and *trans*-dominant PAs, the backbone region is quite planar. Assuming the side-chains attached to both sides of the backbone are coplanar with the main-chain, the SCLCPA can be sheet-like. Our researches demonstrate that for a series of SCLCPAs with a spacer of three methylene units [poly(5-{[(4′-alkyl-4-biphenylyl)carbonyl]oxy}-1-pentyne), P-3,*n*][49] the molecule looks like a sheet as a whole. Several layers of the "sheet" molecules can stack face-to-face forming smectic A (SmA) blocks and the adjacent SmA blocks further glide half the width of "sheet" along the side-chain direction. This packing scheme results in a highly ordered smectic phase (SmX) with the feature of frustrated molecular packing. With a fixed spacer of 3 methylenes, increasing the tail length of the side-chain can change the LC phase from SmX to smectic C (SmC), accompanying with the molecular "sheet" becoming more buckled.

We consider that in the aforementioned SmX of SCLCPAs the short spacer (i.e., three methylene units) is critical, which actually can effectively integrate the PA main-chain and the biphenyl mesogens on side-chain together. In this paper, we study how the variation of spacer length will affect the LC phase of the SCLCPAs. In researches of SCLCPAs, it has been proved that increasing the spacer length can shift the LC phase from nematic (N) to smectic. For example, Tang's work on a series of cyanobiphenyl containing PAs shows that the SCLCPA with a spacer of two methylene units just forms the N phase, while that with eight methylene units as spacer results in the smectic phase.[44] Here, starting from the SmX phase which suggests that the mesogen and backbone are well coupled by short spacer, we will elucidate how many methylene units can cause clearly the decoupling effect by lengthening the spacer. In this case, different from the spacer length effect usually observed, i.e., longer spacer promotes the LC with higher order, we will encounter a change of reducing LC order when lengthening the spacer. The chemical structure of a series of SCLCPAs studied, which are analogue of P-3,*n* mentioned above, is shown in Chart 1 [P-*m*,7 (*m* = 3, 4, 5, 8, 9), P-*m*,5 (*m* = 3, 9), and P-*m*,5^{L} (*m* = 3, 9), *m* denotes the number of methylene units in the spacer]. The phase structures and transitions were investigated mainly by one- and two-dimensional (1D and 2D) wide-angle X-ray diffraction (WAXD). The experimental results indicate that the methylene unit number *m* of 5 is critical in terms of both the molecular shape and phase structure. While the molecules of P-5,7 can retain the sheet-like shape, they no longer pack in the SmX phase but a smectic B (SmB) phase. For *m* > 5, SmB or smectic E (SmE) can be identified. The spacer shall take more gauche conformation and significantly relieve the coupling between the main-chain and side-chain mesogens, making the close packing of biphenyl mesogen possible.

Chart 1. Chemical Structures of the SCLCPAs Studied

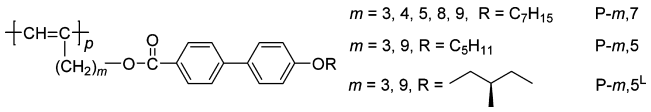

EXPERIMENTAL SECTION

Materials. According to the previous publication,[26] The SCLCPAs with different length of spacer and alkyl tails [P-*m*,7 (*m* = 3, 4, 5, 8, 9), P-*m*,5 (*m* = 3, 9), and P-*m*,5^{L} (*m* = 3, 9)] were synthesized with yield up to 80% by coordination polymerization. To obtain *trans* PA backbone, we selected WCl_6−Ph_4Sn as the catalyst. ^{1}H NMR analysis indicated that all the resultant polymers were of good stereo regularity with the *trans* content of >80%. Molecular characterization of P-3,7, P-4,7, P-9,7, and P-3,5 have been reported previously,[26] while the others are listed in the Supporting Information. Number-average molecular weight and polydispersity of the polymers, which are 3.0−11.0 × 10^4 g/mol and 2.0−3.0, respectively, were measured by gel permeation chromotography (GPC, Waters 150C) calibrated using polystyrene standards. The decomposition temperature determined by thermogravimetric analysis (TGA) at a heating rate of 10 °C/min was higher than 300 °C in a dry nitrogen atmosphere except P-3,5^{L}, which is about 230 °C.

Instruments. Thermal behaviors were examined using differential scanning calorimetry (DSC). Experiments were performed on a NETZSCH 200F3 DSC with a liquid nitrogen refrigerator. The temperatures and heat flows were calibrated using benzoic acid and indium. The phase transition temperatures were determined by measuring the peak temperatures from the cooling/heating scans at a rate of 10 °C/min. 1D WAXD experiments were performed with a Panalytical diffractometer equipped with an X'celerator detector in the reflection mode. 2D WAXD experiments were conducted on a Rigaku Saturn724+ CCD diffractometer (Japan) with an area detector. In the temperature dependent 1D WAXD experiments, the sample temperature was controlled within ±1 °C and the sample was protected by dry nitrogen purge gas during measurements. The X-ray sources (Cu Kα, λ = 0.154 nm) were provided by 3 kW ceramic tubes, and the diffraction peak positions were calibrated with silicon powder (2θ > 15°) and silver behenate (2θ < 10°). The background scattering of WAXD results were recorded and subtracted from the sample patterns. The oriented samples for 2D WAXD measurements were prepared by mechanically shearing from the LC phase, and the point-focused X-ray beam was aligned perpendicular to the mechanical shearing direction. Polarized light microscopy (PLM) experiments were carried out on a Leica DML microscope with a Linkam TP-94 hot stage to observe the LC texture.

RESULTS AND DISCUSSION

Structure Identification of the Low-Temperature Phase. Figures 1a-1f show the PLM images of P-3,5^{L}, P-4,7, P-5,7, P-8,7, P-9,5, and P-9,5^{L}, respectively, which were obtained after the sample cooled from isotropic melt to the indicated temperature following by isothermal annealing. Parts a and b of Figure 1 show the strip-like PLM textures of P-3,5^{L} and P-4,7, while parts c−f show the typical fan-shaped texture

DOI: 10.1021/acs.macromol.5b00692
Macromolecules 2015, 48, 2886−2893

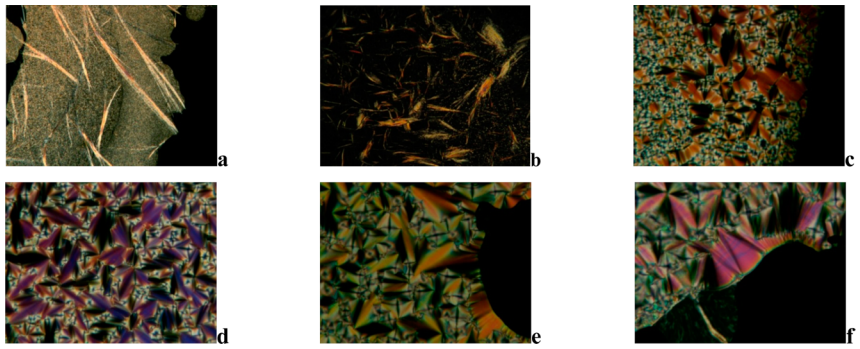

Figure 1. PLM textures recorded after cooling the samples from isotropic melt to the indicated temperature and followed by thermal annealing. Key: (a) P-3,5^{L} at 70 °C; (b) P-4,7 at 70 °C; (c) P-5,7 at 85 °C; (d) P-8,7 at 75 °C; (e) P-9,5 at 75 °C; (f) P-9,5^{L} at 45 °C. Magnification: (a) × 50; (b) × 50; (c) × 200; (d) × 50; (e) × 200; (f) × 200.

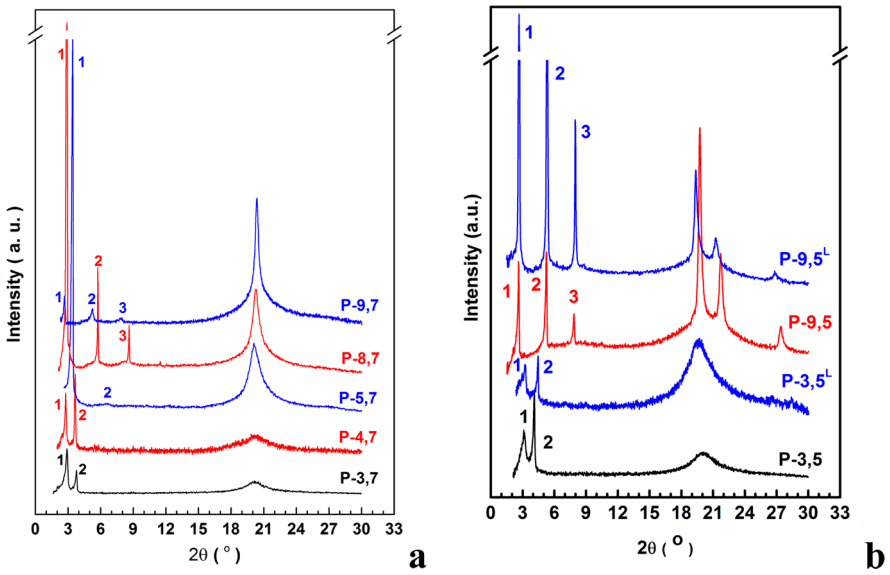

Figure 2. 1D WAXD patterns of (a) P-*m*,7 (*m* = 3, 4, 5, 8, 9); (b) P-*m*,5 and P-*m*,5^{L} (*m* = 3, 9) recorded at room temperature. The patterns of P-3,7 and P-9,7 in (a) and P-3,5 in (b) are plotted here for comparison only.[28,49]

of P-5,7, P-8,7, P-9,5, and P-9,5^{L}. This observation indicates that the SCLCPAs with short spacer length ($m \leq 4$) have the phase structure different from that with long spacer length ($m \geq 5$). While those with $m \leq 4$ form SmX with an addition order on subnanometer scale (SmX^{o}), the samples with $m \geq 5$ form smectic phase with the order higher than SmA, such as SmB or SmE (see below the discussion). In Figure, 1, parts e and f, fan-shaped texture with striation bands can be observed, which is quite readily detected from transition of SmB to SmE phase,[50] indicating there may be a SmE phase formed for P-9,5 and P-9,5^{L}. The phase structures deduced from PLM texture observations would be confirmed by 1D or 2D WAXD experiments.

Figure 2a presents the 1D WAXD patterns of P-*m*,7 (*m* = 3, 4, 5, 8, 9) obtained at room temperature. In agreement with the observation of PLM experiments, the diffraction behavior of $m \geq 5$ is quite different from that of $m \leq 4$. The samples of P-*m*,7 ($m \geq 5$) exhibit a relatively narrow and strong in the high angle region. This single diffraction should be arisen from the ordered packing of biphenyl containing side chains with a hexagonal symmetry. In the low-angle region, P-5,7 presents a strong diffraction at 2θ of 3.42° and meanwhile, a weak diffraction at 2θ of 6.76° can be also recognized. The *q*-ratio ($q = 4\pi\sin\theta/\lambda$, with λ the X-ray wavelength and 2θ the scattering angle) of these two diffractions are of 1:2, suggesting a smectic structure. For P-8,7 and P-9,7, the low-angle diffractions up to the third order following the *q*-ratio of 1:2:3 are clear. Therefore, combining the features of diffractions observed from both the low- and high-angle, we presume that P-*m*,7 ($m \geq 5$) possess the LC phase of SmB. P-4,7 shows the 1D WAXD pattern similar to that of P-3,7 which has been determined to be SmX^{o} in our previous research.[29] The *q*-ratio of low-angle diffractions for P-4,7 is of 1.37, which is far away from the characteristic value 1:2 for the conventional smectic structure. In the high-angle region, P-4,7 renders the scattering narrower than the typical amorphous halo, implying that the side-chains have a sort of order on the subnanometer scale. The 1D WAXD powder patterns of P-*m*,5 or P-*m*,5^{L} (*m* = 3, 9) at room temperature are shown in Figure 2b. The diffraction behavior of P-3,5^{L} is much more similar to that of P-3,5 with the SmX^{o} phase.[29] For P-9,5 and P-9,5^{L}, the *q*-ratios of the strong diffraction peaks in the low-angle region is of 1:2:3. On the other hand, these two samples have three strong and narrow peaks in the high-angle region, which can be assigned to the (10), (11), and (21) diffraction belonging to the side-chain packing with a SmE structure.[51,52]

To verify the low-temperature LC phase of the SCLCPAs inferred from the 1D WAXD results, we performed 2D WAXD

DOI: 10.1021/acs.macromol.5b00692
Macromolecules 2015, 48, 2886−2893

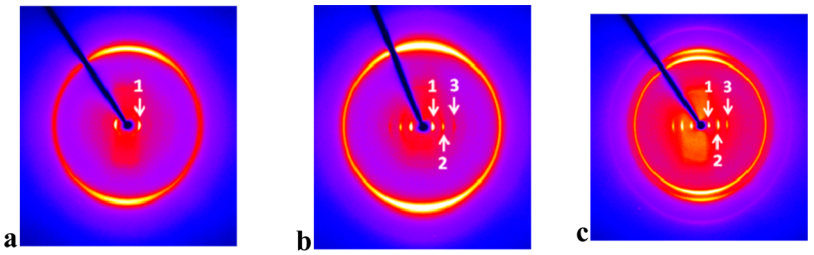

Figure 3. 2D WAXD patterns of oriented (a) P-5,7, (b) P-8,7, and (c) P-9,5 obtained at room temperature. The shear direction is along the meridian and perpendicular to the incident X-ray beam.

Table 1. Low Temperature Phase Structure of SCLCPAs with Different Lengths of Spacer and Alkyl Tail[a]

sample	P-3,7	P-4,7	P-5,7	P-8,7	P-9,7	P-3,5	P-3,5^{L}	P-9,5	P-9,5^{L}
phase structure	SmX^{o}	SmX^{o}	SmB	SmB	SmB	SmX^{o}	SmX^{o}	SmE	SmE

[a]SmX^{o}: highly ordered smectic phase with additional ordering on the subnanometer scale. SmX: highly ordered smectic phase. The phase structures of P-3,7, P-9,7, and P-3,5 were listed for comparison only.[28,49]

experiments of oriented samples. To align the LC domains, the samples were mechanically sheared with mild external force at temperature just below isotropic temperature. The sheared samples were then annealed at properly selected temperatures for several hours, allowing the LC structures to be fully developed. For P-5,7 and P-8,7, the shear temperatures were 140 °C, and the annealing temperatures were 90 and 80 °C, respectively. Figures 3a and 3b describe 2D WAXD patterns of the oriented P-5,7 and P-8,7, respectively, with the incident X-ray beam perpendicular to the shear direction which is along the meridian. As for P-5,7, there observed a pair of strong diffraction spots located at 2θ of 3.42° on the equator. This diffraction indicates that the smectic layer is aligned parallel to the shear direction. When the spacer length was increased to 8 methylene units, three pairs of strong diffraction spots on the equator at 2θ of 2.9, 5.8, and 8.7° can confirm clearly the smectic structure. For both of P-5,7 and P-8,7, a pair of diffraction arcs in the high-angle region, which is quite sharp and strong, is more or less concentrated on the meridian with a *d*-spacing of 0.44 nm. This meridian diffraction indicates that the biphenyl side-chains are packed parallel to the layer normal direction, which is a characteristic of SmB phase. The 2D WAXD pattern of oriented P-9,5 is shown in Figure 3c, wherein the low-angle diffractions are similar to that of P-8,7. In the high-angle region, P-9,5 exhibits three pairs of diffraction arcs on the meridian at 2θ of 19.7°, 21.7°, and 27.4°, respectively, which is typical for SmE phase.[51,52] For P-9,5^{L}, we found that its 2D WAXD pattern was similar to that of P-9,5.

On the basis of the DSC and 1D/2D WAXD results, the phase structure of SCLCPAs studied at low temperature can be well identified, which are summarized in Table 1.

Molecular Packing Behavior of the SCLCPAs at Low Temperature. As shown above, the LC structure of P-*m*,7 exhibits a great change from SmX^{o} to SmB with increasing the spacer length (*m*) at low temperature. To further analyze the molecular packing behavior of P-*m*,7, we shall pay attention to the dimension of the smectic layer structure. Figure 4 gives the *d*-spacing measured from WAXD as functions of *m*, of which the data can be fitted into two linear lines. Note that the *d*-spacings of $m < 5$ presented in Figure 4 correspond to the second order diffraction, while that of $m \geq 5$ are related to the first order diffraction. As indicated by our previous study, SmX^{o} of P-*m*,7 takes the whole sheet-like molecules as the building block, which can parallel stack to form the SmA block.

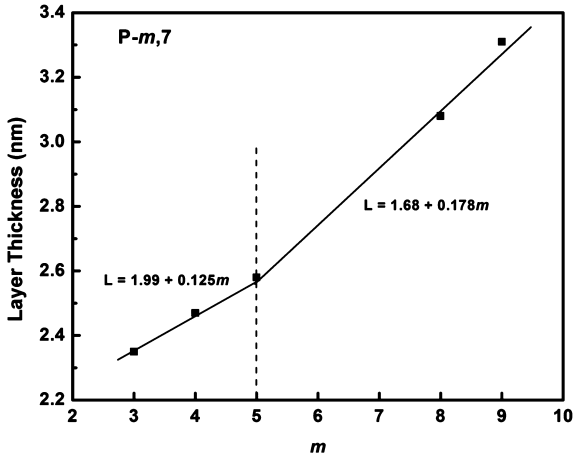

Figure 4. Plot of smectic layer thickness vs the number of methylene units of spacer (*m*). For $m < 5$, the layer thickness corresponds to the *d*-spacing of the second-order diffraction in the low-angle region.

Therefore, the *d*-spacing of the second order diffraction, i.e., the (20) diffraction of SmX^{o}, represents the extended side-chain length. This situation is confirmed by the newly studied sample of P-4,7. The first linear line in Figure 4 possesses the slope of 0.125, evidencing that the methylene sequence of the samples with SmX^{o} phase adopts an all-*trans* conformation. For $m \geq 5$, Figure 4 illustrates that *d*-spacings of the first order diffraction also fairly follows a linear line with the slope of 0.178. While the measured layer period of P-8,7 is still close to the extended side-chain length (3.08 nm vs 3.03 nm), the difference between the layer period and side-chain length becomes larger at $m = 9$ (3.31 nm vs 3.15 nm). The outcome suggests that P-8,7 and P-9,7 have a monolayer smectic structure, and with longer spacer the side-chains are packed partially interdigitated. The well-developed SmB phase indicates the biphenyl mesogen are packed rather closely. According to the high-angle diffraction observed, the parameter of hexagonal lattice of the biphenyl (a') is of 0.51 nm, in agreement with that reported in the literature.[51] Having an ester moiety attached at one end, the biphenyl group on the side-chain possesses a dipole moment, which in fact favors more the interdigitated packing. Considering that the biphenyl groups insert into the SmB layer from both sides, there are two sublayers of spacers involved in the smectic layer. Therefore, half the slope (0.089 =

DOI: 10.1021/acs.macromol.5b00692
Macromolecules 2015, 48, 2886−2893

Chart 2. Schematic of Molecular Size of (a) P-5,7 and (b) P-9,7

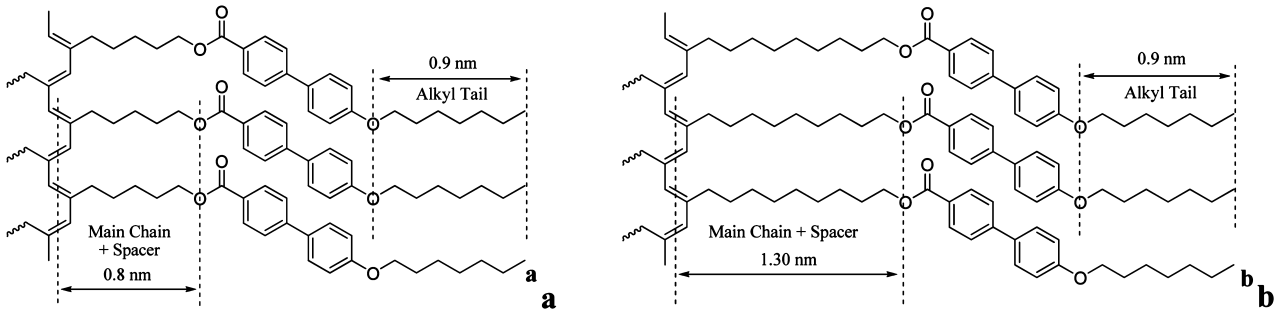

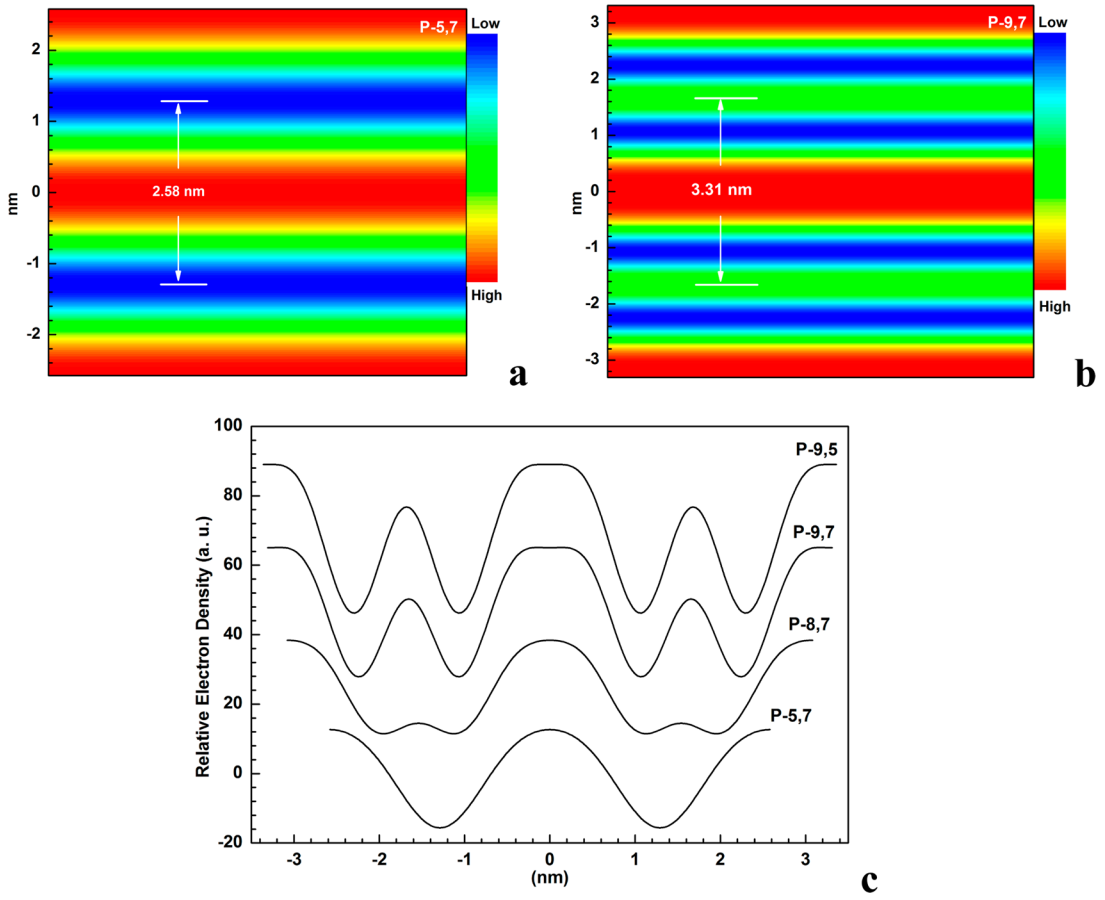

Figure 5. Relative electron density maps reconstructed based on the 1D WAXD results of (a) P-5,7 and (b) P-9,7. (c) One-dimensional relative electron density profiles of P-*m*,7 (*m* = 5, 8, 9) and P-9,5 along the smectic layer normal, which demonstrate that increasing *m* will facilitate the phase separation within the smectic layer.

0.178/2) smaller than that of 0.125 implies that the alkyl spacers of P-8,7 and P-9,7 adopt more *gauche* conformations.

It is important to note that the layer spacing of P-5,7 with the SmB phase clearly evidenced by WAXD results is also on the linear line with the slope of 0.125. This suggests that the side-chain of P-5,7 is still fully extended. Assuming the spacer and tails of P-5,7 are in all-*trans* conformation, detailed calculation can elucidate that the length of tail is comparable to the combined length of "main-chain + spacer" (Chart 2), of which the difference is only 0.1 nm. In this case, when packed into the smectic structure, the molecules of P-5,7 can retain the sheet-like shape as a whole. The "sheet" molecules can either fully parallel stack or fully interdigitated pack with each other, wherein the latter one can be considered as that the molecular "sheet" glides half the width along the side-chain direction. When the "sheet" molecules of P-5,7 adopt randomly the two packing manners in the smectic phase, the maximization of intermolecular interaction and packing entropy can be satisfied simultaneously, and thus the SmX^{o} structure becomes unnecessary.

Concerning where the decoupling between backbone and mesogens on side-chains will occur in P-*m*,7, we consider that *m* = 5 is critical. In our previous study,[49] we find that with the spacer length fixed at *m* = 3, increasing the tail length will result in the LC phase change from SmX^{o} to SmC. As the short spacer tightly links the PA backbone and biphenyl, the sheet-like shape is rather persistent. In the SmC phase of P-3,11, to maximize the intermolecular interaction between biphenyl mesogens, the buckled "sheets" are stacked parallel to each other.[49] For P-*m*,7 with *m* > 5, the mismatch between the

DOI: 10.1021/acs.macromol.5b00692
Macromolecules 2015, 48, 2886−2893

Table 2. Phase Transition Temperatures Determined by DSC[a]

	heating	cooling
P-3,7	SmXo 98 SmX 162 SmC 175 Iso	SmXo 94 SmX 157 SmC 166 Iso
P-4,7	SmXo 75 SmX 140 SmC 151 Iso	SmXo 75 SmX 131 SmC 140 Iso
P-5,7	SmB 91 SmA 144 Iso	SmB 88 SmA 136 Iso
P-8,7	SmB 81 SmA 146 Iso	SmB 79 SmA 140 Iso
P-9,7	SmB 70 SmA 118 Iso	SmB 66 SmA 115 Iso
P-3,5	SmXo 113 SmX 180 SmC 193 Iso	SmX^{o} 104 SmX 170 SmC 179 Iso
P-9,5	SmE 82 SmB 92 SmA 134 Iso	SmE 73 SmB 89 SmA 130 Iso
P-3,5^{L}	SmXo 73 SmX 113 SmC 154 Iso	SmX^{o} 70 SmX 106 SmC 136 Iso
P-9,5^{L}	SmE 49 SmB 63 SmA 105 Iso	SmE 42 SmB 62 SmA 102 Iso

[a]The data are obtained in °C from the peaks of heating (left) and cooling (right) scan at a rate of 10 °C/min.

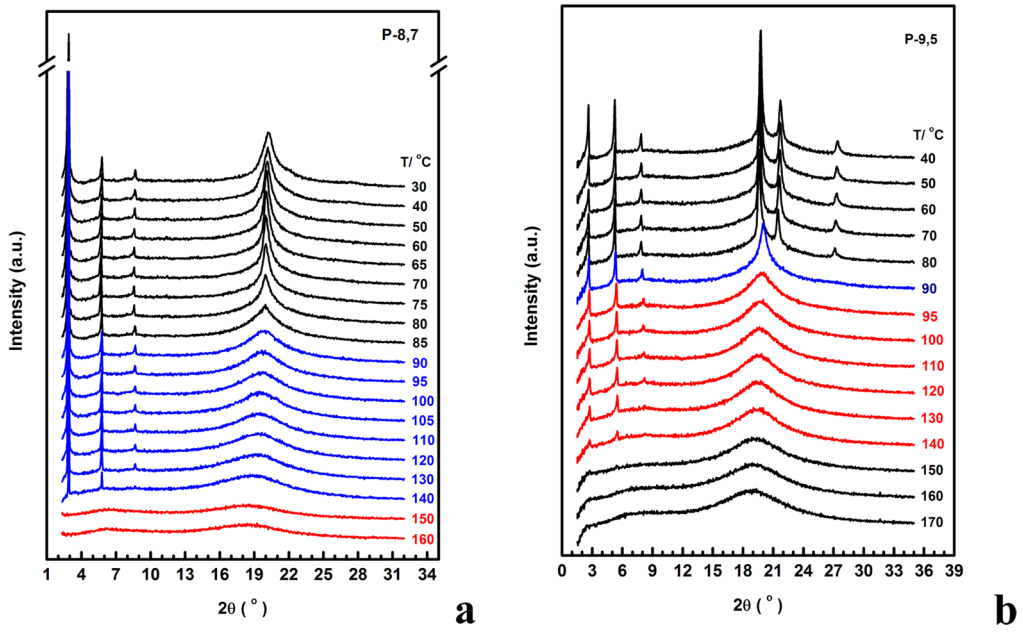

Figure 6. Sets of 1D WAXD patterns of P-8,7 (a) and P-9,5 (b) obtained during heating.

lengths of tail and spacer becomes significant (as an example, see P-9,7 in Chart 2). However, as the longer spacer can take more *gauche* conformation, the effective length of spacer can be flexibly adjusted. Furthermore, this spacer conformation variation also allows the biphenyl groups to move more freely. Consequently, the LC order higher than SmA, i.e., SmB, can be realized, exemplifying clearly the decoupling effect arisen from the flexible spacer.

For the SmB of P-*m*,7 observed, we find that the molecular packing within the smectic layer is also influenced by variation of *m*. As shown in Figure 2, in the low-angle region, P-5,7 gives the first order diffraction with the intensity 110 times larger than that of the second one. With increasing *m*, the intensity ratio of the first to second order diffraction decreases, suggesting that the electron density distribution within the smectic layer is varied. Parts a and b of Figure 5 describe the relative electron density maps reconstructed based on the 1D WAXD result of P-5,7 and P-9,7, respectively. For both samples, it is reasonable to assign the high electron density zone (red colored) with the dimension of ∼0.9 nm to the biphenyl groups. However, compared with that of P-5,7, the electron density map of P-9,7 looks more complex. Figure 5c describes the 1D electron density profiles along the smectic layer normal of the P-*m*,7 ($m \geq 5$). For P-5,7, only one maximum and one minimum of electron density can be observed, which should be associated with the fully interdigitated packing behavior. However, a maximum in addition to that corresponding to the biphenyl zone can be observed in P-8,7, which becomes clearer in P-9,7. According to the chemical structure and the partially interdigitated packing model of smectic phase, this additional maximum shall reflect the packing of main-chains. The increase of *m* can result in more completed microphase separation within the smectic layer. For $m > 5$ (particularly for $m = 9$), three different sublayers, which are rich in the biphenyl, the aliphatic, and the main-chain, respectively, can be identified. From Figure 2a, we also observe that in the high-angle region the characteristic diffraction of SmB becomes narrower with increasing *m*. Using Scherrer's relation, we estimated the apparent correlation length perpendicular to the long axis of the hexagonally packed biphenyl, which increases from 6.3 to 9.6 to 17.1 nm when *m* increases from 5 to 8 to 9. Therefore, the longer and more flexible spacer facilitates better SmB structure.

Considering that with $m = 9$ the spacer can afford the rod-like mesogen of biphenyl pretty large mobility, we intended to see if a chiral center attached to the end of biphenyl would induce a chiral LC phase and the sample of P-9,5^{L} was thusly synthesized. Akagi et al. have introduced fluorine containing chiral LC group to the side-chain of polyacetylene or polythiophene and obtained monotropic or enantiotropic chiral

DOI: 10.1021/acs.macromol.5b00692
Macromolecules 2015, 48, 2886−2893

LC phase (SmC* or TGBA*).[32,53] However, probably due to that the chiral 2-methyl-1-butyl group is small and the parallel packing of biphenyl dominates phase structure, P-9,5^{L} cannot form chiral LC phase, but exhibits SmE phase at room temperature, wherein the biphenyl groups packed in a rectangular lattice with a' = 0.84 nm and b' = 0.55 nm. The SmE phase can be also seen in P-9,5. Seemingly, shortening the tail can promote the self-organization of biphenyl groups, and thus the SmE structure which is more ordered than SmB can be achieved.

Phase Transition Behaviors. DSC experiments were applied to investigate the phase transitions. The results show that all the transitions are enantiotropic. The DSC cooling and subsequent heating traces of P-m,7 (m = 4, 5, 8), P-9,5, and P-m,5^{L} (m = 3, 9) at a cooling/heating rate of 10 °C/min are shown in Figure S1 and the phase transition temperatures are listed in Table 2, of which some of the previously reported data are listed for comparison. The results show that the temperature of the first transition during heating decreases from 98 °C for P-3,7 to 70 °C for P-9,7 and the transition temperature of P-3,5^{L} and P-9,5^{L} is 30−40 °C lower than that of P-3,5 and P-9,5, respectively.

We confirmed the phase transitions by temperature dependent 1D WAXD experiments. The structural evolution of P-4,7 and P-3,5^{L} during heating are shown in Figure S2, which is similar to that of the previously reported P-3,7 and P-3,5, respectively.[49] The phase transition sequence for both of P-4,7 and P-3,5^{L} are SmX^{o} ↔ SmX ↔ SmC ↔ Iso. As for the samples with $m \geq 5$, the phase transition behaviors were different from that of P-4,7. Here, we select P-8,7 as an example to analyze the phase transition process. Figure 6a shows the thermal 1D WAXD results of P-8,7. At below 85 °C, the sample forms SmB phase as discussed above. When the temperature was increased to higher than 85 °C, the diffraction peak in the high-angle region broadens to be a scattering halo and on the other hand, the low-angle diffraction behavior changes little, suggesting that the SmB phase transforms to SmA which corresponds to the low temperature transition detected by DSC. When the temperature exceeded 140 °C, the scattering halo in the high angle region continually broadens and slightly shifts to lower angle. Meanwhile, the diffractions in the low-angle region completely disappear. The two amorphous halos observed in both low- and high-angle region indicate an isotropic melt of P-8,7, which corresponds to the high temperature transition. On the basis of the DSC and 1D WAXD results, we conclude that the phase transition sequence of P-m,7 ($m \geq 5$) is SmB ↔ SmA ↔ Iso.

For P-9,5, the phase transition behavior is different from that P-m,7, as it can form a SmE phase at low temperatures. The 1D WAXD patterns of P-9,5 recorded upon heating is depicted in Figure 6b. For the diffractions shown in the high-angle region, when the temperature reached 90 °C, the peak at 2θ of 19.7° slightly shifts to 20° and the other two disappear, indicating the transition from SmE to SmB. Upon heating to 95 °C, the high-angle diffraction of SmB changes to a scattering halo, corresponding to the second transition observed during DSC heating which should be the transformation of SmB to SmA. For the low-angle region, the three strong peaks become slightly weaker when the temperature became higher than 95 °C. Once they are destroyed at above 140 °C, the sample enters isotropic melt. The summarized phase transition of P-9,5 is SmE ↔ SmB ↔ SmA ↔ Iso. The thermal 1D WAXD result of P-9,5^{L} is shown in Figure S3, which is very similar to that of P-9,5 except the decreased transition temperature and slightly shifted diffraction peak positions.

On the basis of the WAXD results of phase transitions, the parameters of LC structures of the SCLCPAs with short ($m \leq 4$) and long spacers ($m \geq 5$) are listed in Table 3.

Table 3. Side-Chain Length and Lattice Dimensions of LC Structures of the SCLCPAs

for short spacers ($m \leq 4$)					
		SmX^{o}		SmC	
	l_{SC} (nm)[a]	a (nm)[b]	b (nm)[b]	layer period (nm)	tilt angle (deg)
P-3,7[c]	2.40	4.80	4.40	3.40	45
P-4,7	2.53	4.95	4.42	3.02	45
P-3,5^{L}	2.03	3.96	3.74	3.40	45
P-3,5[c]	2.15	4.35	3.55	3.93	48

for long spacers ($m \geq 5$)					
			SmE		SmB
	l_{SC} (nm)[a]	layer period (nm)	a' (nm)[d]	b' (nm)[d]	a' (nm)[e]
P-5,7	2.65	2.58			0.51
P-8,7	3.03	3.08			0.51
P-9,7[c]	3.15	3.31			0.51
P-9,5	2.90	3.36	0.82	0.54	0.51
P-9,5^{L}	2.78	3.31	0.84	0.55	0.52

[a]Estimated extended side-chain length. [b]Parameter of the 2D rectangular lattice for the SmX^{o} structure. [c]The published data listed here for comparison only. [d]Parameter of the 2D rectangular lattice for the side chains within the SmE layer. [e]Parameter of the 2D hexagonal lattice for the side chains within the SmB layer.

CONCLUSION

In summary, we have investigated the phase structures and transitions of a series of biphenyl containing SCLCPAs (P-m,7, P-m,5, and P-m,5^{L}) with different length of spacers using PLM, DSC, 1D- and 2D-WAXD. We confirm that with shorter spacers the SCLCPAs (m < 5) studied can form a highly ordered SmX^{o} phase at low temperatures. In this case, the (semi)rigid PA backbone and mesogenic groups on side-chains are tightly coupled together, forming a sheet-like molecular structure which acts as the building block of LC phase. For m > 5, P-m,7 forms SmB phase at low temperatures, while P-9,5 and P-9,5^{L} form SmE. As the interdigitated packing of biphenyl groups dominates the LC phase structure, the long spacers have to take more *gauche* conformations. This makes the molecular shape no longer sheet-like as a whole, and the backbone and main-chain are decoupled. In this work, we emphasize that the spacer length of m = 5 is critical. The SmB layer period of P-5,7 determined by WAXD is almost identical to the extended side-chain length, suggesting the molecule remains the sheet-like feature. However, the P-5,7 molecules can fully interdigitated pack together to form a SmB rather than a SmX^{o}. We find that all the samples studied here exhibit enantiotropic LC phase behavior. The SCLCPAs with m < 5 present a SmC phase after their SmX are melted upon heating. For m > 5, the side-chains can remain perpendicular to the smectic layer surface until the isotropization occurred at high temperatures. This observation also reflects the impact of varying spacer length. Starting from different low temperature LC phases which are determined by whether the main- and side-chain are coupled, the phase transition sequences can be very different.

DOI: 10.1021/acs.macromol.5b00692
Macromolecules 2015, 48, 2886−2893

■ ASSOCIATED CONTENT

Supporting Information

Structural characterization data of P-*m*,7 (*m* = 5, 8), P-9,5, and P-*m*,5^{L} (*m* = 3, 9); method of electron density reconstruction and electron density profiles of P-8,7 and P-9,5; DSC traces of P-*m*,7 (*m* = 4, 5, 8), P-9,5, and P-*m*,5^{L} (*m* = 3, 9); and sets of 1D WAXD powder patterns of P-*m*,7 (*m* = 4, 5) and P-*m*,5^{L} (*m* = 3, 9). This material is available free of charge via the Internet at http://pubs.acs.org.

■ AUTHOR INFORMATION

Corresponding Authors

*E-mail: zqyu@szu.edu.cn (Z.Q.Y.).
*E-mail: eqchen@pku.edu.cn (E.Q.C.).
*E-mail: tangbenz@ust.hk (B.Z.T.).

Notes

The authors declare no competing financial interest.

■ ACKNOWLEDGMENTS

This work was partially supported by the National Natural Science Foundation of China (21074073, 51273002) and Shenzhen Science and Technology Bureau (JCYJ20140418193546112).

■ REFERENCES

(1) Finkelmann, H.; Happ, M.; Portugal, M.; Ringsdorf, H. *Macromol. Chem.* **1978**, *179*, 2541−2544.
(2) Finkelmann, H.; Ringsdorf, H.; Wendorff, H. *Makromol. Chem.* **1978**, *179*, 273−276.
(3) Liu, J. Z.; Lam, J. W. Y.; Tang, B. Z. *Chem. Rev.* **2009**, *109*, 5799−5867.
(4) Akagi, K. *Chem. Rev.* **2009**, *109*, 5354−5401.
(5) Lam, J. W. Y.; Tang, B. Z. *J. Polym. Sci., Part A: Polym. Chem.* **2003**, *41*, 2607−2629.
(6) Lam, J. W. Y.; Tang, B. Z. *Acc. Chem. Res.* **2005**, *38*, 745−754.
(7) Aoki, T.; Kaneko, T.; Teraguchi, M. *Polymer* **2006**, *47*, 4867−4892.
(8) Nagai, K.; Masuda, T.; Nakagawa, T.; Freeman, B. D.; Pinnau, I. *Prog. Polym. Sci.* **2001**, *26*, 721−798.
(9) Choi, S. K.; Gal, Y. S.; Jin, S. H.; Kim, H. K. *Chem. Rev.* **2000**, *100*, 1645−1682.
(10) Hu, Y. M.; Hattori, K.; Fukui, A.; Shiotsuki, M.; Sanda, F.; Masuda, T. *Polymer* **2010**, *51*, 1548−1554.
(11) Hu, Y. M.; Shiotsuki, M.; Sanda, F.; Freeman, B. D.; Masuda, T. *Macromolecules* **2008**, *41*, 8525−8532.
(12) Kumaki, J.; Sakurai, S.; Yashima, E. *Chem. Soc. Rev.* **2009**, *38*, 737−746.
(13) Zhang, D. Y.; Song, C.; Deng, J. P.; Yang, W. T. *Macromolecules* **2012**, *45*, 7329−7338.
(14) Li, B. S.; Cheuk, K. K. L. L.; Ling, S.; Chen, J. W.; Xiao, X. D.; Bai, C. L.; Tang, B. Z. *Macromolecules* **2003**, *36*, 77−85.
(15) Li, B. S.; Lam, J. W. Y.; Yu, Z. Q.; Tang, B. Z. *Langmuir* **2012**, *28*, 5770−5774.
(16) Wang, X.; Yan, Y. X.; Liu, T. B.; Su, X. Y.; Qian, L. W.; Song, Y. L.; Xu, H. Y. *J. Polym. Sci., Part A: Polym. Chem.* **2010**, *48*, 5498−5504.
(17) Li, Z. A.; Yu, G.; Wu, W. B.; Liu, Y. Q.; Ye, C.; Qin, J. G.; Li, Z. *Macromolecules* **2009**, *42*, 3864−3868.
(18) San, J. B. A.; Akagi, K. *Polym. Chem.* **2013**, *4*, 5144−5161.
(19) San, J. B. A.; Matsushita, S.; Akagi, K. J. *Am. Chem. Soc.* **2012**, *134*, 19795−19807.
(20) Liu, X. Q.; Li, Y. L.; Lin, Y. W.; Yang, S.; Guo, X. F.; Li, Y.; Yang, J.; Chen, E. Q. *Macromolecules* **2013**, *46*, 8479−8487.
(21) Meyer, N. C.; Krupp, A.; Schmidts, V.; Thiele, C. M.; Reggelin, M. *Angew. Chem., Int. Ed.* **2012**, *51*, 8334−8338.
(22) Liu, K. P.; Yu, Z. Q.; Chen, E. Q. *Macromol. Chem. Phys.* **2009**, *210*, 708−716.
(23) Ting, C. H.; Chen, J. T.; Hsu, C. S. *Macromolecules* **2002**, *35*, 1180−1189.
(24) Stagnaro, P.; Conzatti, L.; Costa, G.; Gallot, B.; Valenti, B. *Polymer* **2003**, *44*, 4443−4454.
(25) Zhou, D.; Chen, Y. W.; Chen, L.; Zhou, W. H.; He, X. H. *Macromolecules* **2009**, *42*, 1454−1461.
(26) Lam, J. W. Y.; Kong, X.; Dong, Y.; Cheuk, K. K. L.; Xu, K.; Tang, B. Z. *Macromolecules* **2000**, *33*, 5027−5040.
(27) Geng, J.; Zhao, X.; Zhou, E.; Li, G.; Lam, J. W. Y.; Tang, B. Z. *Mol. Cryst. Liq. Cryst.* **2003**, *399*, 17−28.
(28) Yu, Z. Q.; Liu, J. H.; Zhu, C. Z.; Chen, E. Q.; Tang, B. Z. *Acta Polym. Sin.* **2010**, 783−788.
(29) Ye, C.; Xu, G. Q.; Yu, Z. Q.; Lam, J. W. Y.; Jang, J. H.; Peng, H. L.; Tu, Y. F.; Liu, Z. F.; Jeong, K. U.; Cheng, S. Z. D.; Chen, E. Q.; Tang, B. Z. *J. Am. Chem. Soc.* **2005**, *127*, 7668−7669.
(30) Kong, X.; Tang, B. Z. *Chem. Mater.* **1998**, *10*, 3352−3363.
(31) Stagnaro, P.; Cavazza, B.; Trefiletti, V.; Costa, G.; Gallot, B.; Valenti, B. *Macromol. Chem. Phys.* **2001**, *202*, 2065−2073.
(32) Goto, H.; Dai, X.; Ueoka, T.; Akagi, K. *Macromolecules* **2004**, *37*, 4783−4793.
(33) Kuroda, H.; Goto, H.; Akagi, K.; Kawaguchi, A. *Macromolecules* **2002**, *35*, 1307−1313.
(34) Yu, Z. Q.; Lam, J. W. Y.; Zhao, K. Q.; Zhu, C. Z.; Yang, S.; Lin, J. S.; Li, B. S.; Liu, J. J.; Chen, E. Q.; Tang, B. Z. *Polym. Chem.* **2013**, *4*, 996−1005.
(35) Okoshi, K.; Sakurai, S. I.; Kumaki, J.; Yashima, E. *Macromolecules* **2005**, *38*, 4061−4064.
(36) Percec, V.; Rudick, J. G.; Peterca, M.; Wagner, M.; Obata, M.; Mitchell, C. M.; Cho, W. D.; Balagurusamy, V. S. K.; Heiney, P. A. *J. Am. Chem. Soc.* **2005**, *127*, 15257−15264.
(37) Percec, V.; Aqad, E.; Peterca, M.; Rudick, J. G.; Lemon, L.; Ronda, J. C.; De, B. B.; Heiney, P. A.; Meijer, E. W. *J. Am. Chem. Soc.* **2006**, *128*, 16365−16372.
(38) Percec, V.; Rudick, J. G.; Wagner, M.; Obata, M.; Mitchell, C. M.; Cho, W. D.; Magonov, S. N. *Macromolecules* **2006**, *39*, 7342−7351.
(39) Sakurai, S. I.; Okoshi, K.; Kumaki, J.; Yashima, E. *Angew. Chem., Int. Ed.* **2006**, *45*, 1245−1248.
(40) Sakurai, S. I.; Okoshi, K.; Kumaki, J.; Yashima, E. *J. Am. Chem. Soc.* **2006**, *128*, 5650−5651.
(41) Okoshi, K.; Kajitani, T.; Nagai, K.; Yashima, E. *Macromolecules* **2008**, *41*, 258−261.
(42) Sakurai, S. I.; Okoshi, K.; Kumaki, J.; Yashima, E. *J. Am. Chem. Soc.* **2006**, *128*, 5650−5651.
(43) Peng, H. X.; Chen, Y. W.; Chen, L.; He, X. H.; Li, F. *J. Polym. Sci., Part A: Polym. Chem.* **2010**, *48*, 5679−5692.
(44) Tang, B. Z.; Kong, X. X.; Wan, X. H.; Peng, H.; Lam, J. W. Y.; Feng, X. D.; Kwok, H. S. *Macromolecules* **1998**, *31*, 2419−2432.
(45) Chen, Y. W.; Kong, H. L.; Chen, L.; Qin, Z. Y.; Zhou, W. H.; Li, F.; He, X. H. *Synth. Met.* **2009**, *159*, 2049−2055.
(46) Liu, X. Q.; Wang, J.; Yang, S.; Chen, E. Q. *ACS Macro. Lett.* **2014**, *3*, 834−838.
(47) Percec, V.; Rudick, J. G.; Peterca, M.; Aqad, E.; Imam, M. R.; Heiney, P. A. *J. Polym. Sci., Part A: Polym. Chem.* **2007**, *45*, 4974−4987.
(48) Percec, V.; Peterca, M.; Rudick, J. G.; Aqad, E.; Imam, M. R.; Heiney, P. A. *Chem.—Eur. J.* **2007**, *13*, 9572−9581.
(49) Yu, Z. Q.; Lam, J. W. Y.; Zhu, C. Z.; Yang, S.; Chen, E. Q.; Tang, B. Z. *Macromolecules* **2013**, *45*, 588−596.
(50) Dierking, I. *Textures of Liquid Crystals*; Wiley-VCH Verlag: Weinheim, Germany, 2003.
(51) Park, S.-Y.; Zhang, T.; Interrante, L. V.; Farmer, B. L. *Macromolecules* **2002**, *35*, 2776−2783.
(52) Xie, H. L.; Jie, C. K.; Yu, Z. Q.; Liu, X. B.; Zhang, H. L.; Shen, Z. H.; Chen, E. Q.; Zhou, Q. F. *J. Am. Chem. Soc.* **2010**, *132*, 8071−8080.
(53) Goto, H.; Dai, X. M.; Narihiro, H.; Akagi, K. *Macromolecules* **2004**, *37*, 2353−2362.

DOI: 10.1021/acs.macromol.5b00692
Macromolecules 2015, 48, 2886−2893